Available online at www.sciencedirect.com
ScienceDirect
Physica C 452 (2007) 21–28
PHYSICA C
www.elsevier.com/locate/physc

Vacuum heat treatment effect on the thermophysical properties of BSCCO system

S.M. Khalil *, A.M. Ahmed

Physics Department, Faculty of Science, South Valley University, Sohag, Egypt

Received 29 August 2006; received in revised form 21 November 2006; accepted 21 November 2006
Available online 17 January 2007

Abstract

Vacuum heat treatment effects at 850 °C for (3, 6, 9 and 12 h) on the crystalline structure and superconducting, as well as on the mechanical properties of $Bi_4Sr_3Ca_3Cu_6O_x$ (BSCCO) have been studied. The highest critical transition temperature T_c 102 K was achieved at annealing time $t_{ann} = 9$ h. This maximum value is attributed to movement of excess oxygen from annealed sample. Phase examination by X-ray diffraction (XRD) revealed that the gradual formation of the high-T_c phase (2223) due to the prolongation of annealing time up to 9 h. Thereafter, the high-T_c phase starts degrading and T_c reduces. The distortion of the 2223 phase is suggested by the broadening of the different XRD peaks. Also, at the same above annealing time (9 h), SEM observation shows good quality plate-like crystal with relatively oriented. On the other hand, the Vickers microhardness (VHN) measurements was found to be dependent on the annealing conditions, a tremendously increase of VHN value 1.92 GPa (0.25 N) at $t_{ann} = 9$ h. This substantial increase is ascribed to improvement of the thermal conduction and stabilization of temperature distribution between superconducting grains.

Keywords: $Bi_4Sr_3Ca_3Cu_6O_x$; Vacuum heat treatment; High-T_c phase (2223); Low-T_c phase (2212); Microhardness; Density

1. Introduction

Since the discovery [1,2] of high-T_c superconductivity in bismuth-based oxide systems which did not contain any rare-earth element (BiSrCaCuO), great efforts have been focused [3,4] on the study of the structural, electronic, and mechanical properties of the superconducting phases. Whereas the system contains basically two high-T_c phases, one is the low-T_c (~80 K) 2212 and the other is the high-T_c phase (~110 K) 2223 phase, it is extremely difficult to synthesize 2223 in single phase from $Bi_2Sr_2Ca_2Cu_3$ alone.

The annealing process is one of the important methods to accelerate the formation of the 2223 phase [5,6]. Khalil [5] reported that the T_c increment from 93 K to 113 K obtained by atmosphere annealing of $Bi_{1.72}Pb_{0.78}Sr_2Ca_2Cu_3O_y$ specimens was due to an increase in the volume fraction of the high-T_c (2223) phase. On the other hand, another report of the interdependence of T_c on the oxygen stoichiometry of the superconducting phases was shown by Bahadur et al. [7]. They concluded that the enhancement of T_c obtained by thermal treatment was due to oxygen deficiency.

A variety of methods [4,8–10], including oxidation and deoxidation effects, have been employed to change the oxygen content in Bi-based superconductors. The lowest T_c value of 63 K was reported by Sarker and Maartese [4] after oxygen annealing, whereas an enhancement of T_c has been accomplished by vacuum annealing [8,11–13]. Therefore, there is an ample interest in investigating the effect of vacuum annealing on the superconducting properties of $Bi_4Sr_3Ca_3Cu_6O_x$ samples.

On the other hand, since the BSCCO phases have a plate-like morphology with a high current carrying capacity in the *a–b* plane and also owing to the importance of this system, researchers around the world have been trying to develop the practical application potential of it. Most

* Corresponding author. Tel.: +20 934674818; fax: +20 934601950.
E-mail address: khalil_20002000@yahoo.com (S.M. Khalil).

0921-4534/$ - see front matter © 2006 Elsevier B.V. All rights reserved.
doi:10.1016/j.physc.2006.11.011

applications require both desirable superconducting properties (T_c, upper critical magnetic field H_{C2} and critical current density J_c) and mechanical integrity (fracture toughness K_{IC}, ductility, and Vickers hardness VHN). Previous authors have observed that the BSCCO systems are generally brittle with unacceptably low strength [14,15]. In order to solve this problem, we must understand how processing controls the interaction between superconducting and mechanical properties.

In view of this problem, efforts have been made to improve J_c and the mechanical properties of the BSCCO system. Khalil [16] recently reported a K_{IC} value of 0.013 MPa $\sqrt{m}$ for $Bi_2Sr_2Ca_2Ba_{0.45}Cu_5O_y$. Also, Young's modulus (E) registered a considerable practical value of 26.6 GPa for $Bi_{1.7}Pb_{0.3}Sr_2Ca_2Cu_3O_y$ [17].

For commercially useful applications, several processing techniques are under consideration. These includes doping [16], partial substitution [17–19], and atmospheric annealing [3,5]. Here, we report a developed processing technique that has greatly improved the mechanical characteristics of BSCCO samples without adversely affecting the superconducting properties (T_c). This technique is known as "vacuum annealing treatment". In this circumstance, it is of interest to investigate the effects of vacuum annealing on the physical properties of $Bi_4Sr_3Ca_3Cu_6O_x$ samples in order to examine the changes that occur in the samples for different annealing time.

2. Experimental

Bulk superconducting materials with nominal composition $Bi_4Sr_3Ca_3Cu_6O_x$ were fabricated by means of a ceramic solid state–state diffusion reaction. Fine powders of Bi_2O_3, $SrCO_3$, $CaCO_3$ and CuO with purities of more than (99.999%) with appropriate cationic ratio were weighed, thoroughly mixed and ground, and calcined in air at 800 °C for 18 h. The reacted material was then reground and cold pressed into disks or pellets by applying a pressure of 5 ton/cm^2 using a cylindrical die made of stainless steel. Afterwards, the pellets were additionally sintered in air at 850 °C for 100 h. At the end of the sintering process the pellets were allowed to furnace-cool to room temperature. The vacuum annealing conditions of the samples were set at a constant temperature of 850 °C under 0.01 Torr for 3, 6, 9 and 12 h. At the end of each step of the vacuum annealing process the samples were studied for their electrical and structural properties. Identification of various phases present in the samples was done on the basis of the characteristics of their XRD peaks. X-ray diffraction patterns were recorded with CuKα radiation on a Schamdzu X-ray diffractometer.

The temperature dependence of the electrical resistivity was measured by the standard four-point probe technique in the temperature range 77–300 K. Electrical contacts were made with silver paint curable at room temperature. The microstructure was investigated with a JEOL scanning electron microscope (SEM) Model JSM-5300. The samples were coated with a thin layer of gold to avoid the charging effect. Physical density measurements were performed by Archimedes method.

To study the mechanical properties of vacuum annealed BSCCO material, Vickers microhardness was measured using an E. Ltd. Wetzlar microhardness tester with pyramid indenter. A pyramid indenter was employed in all the microhardness tests because it does not penetrate as deeply into the surface, thereby causing less cracking around the indentations. The contact loads (P) ranged from 300 gf (2.490 N) to 25 gf (0.245 N) for the examined samples. A loading time of 15 s was used to measure the diagonal of indentation with an accuracy of ± 0.1 μm. An average of 10 indentations at different locations on the specimen surface was done to obtain representative mean values for each load.

The Vickers microhardness values (VHN) were determined using the following equation:

$$\mathrm{VHN} = 1.8544(P/d^2) \quad (1)$$

where "P" is the applied load in N and "d" is the diagonal length of the indentation mark in mm.

3. Experimental results and discussion

3.1. XRD analysis

The formation of different phases at various stages of vacuum annealing time has been made evident by the investigations of the XRD patterns. These studies also bring about the mechanism of growth of the high-T_c phase in the annealed sample. Fig. 1(a)–(d) illustrates the variation of X-ray patterns for the $Bi_4Sr_3Ca_3Cu_6O_x$ sample as-sintered and vacuum annealed at 850 °C for (6, 9, and 12 h, respectively). H an L in this figure indicate the high-T_c (2223) and low-T_c (2212) phase, respectively. Other identified phases are written in terms of their chemical formula and denoted directly on the diffractograms above their corresponding peaks. For the as-sintered sample in Fig. 1(a), it can be seen that the majority of the peaks are due to the high-T_c (2223) phase, while a minority of the peaks belong to low-T_c (2212) phase. Some indications of formation of CuO with characteristic diffraction peak at $2\Theta = 38.4°$ is present. Fig. 1(b), at relatively short time of vacuum annealing, e.g., 6 h, one can easily observe that the diffraction peaks corresponding to the high-T_c phase and the low-T_c phase have been found to develop with gradually increasing intensity. The impurity peak due to secondary phase CuO remains nearly the same. For 9 h of annealing time with the maximum value of $T_c = 102$ K, the peaks corresponding to the low-T_c phase have slightly decreased at $2\Theta = 23.2°$ and 29.1°, as can be seen in the XRD patterns of Fig. 1(c). Most of peaks could be assigned to the high-T_c phase, i.e., the high-T_c phase dominates the phase maximum. This affirmative observation may be due to enhancement of outgoing oxygen from the annealed sample. Hence, this loss of oxygen favors the formation of the

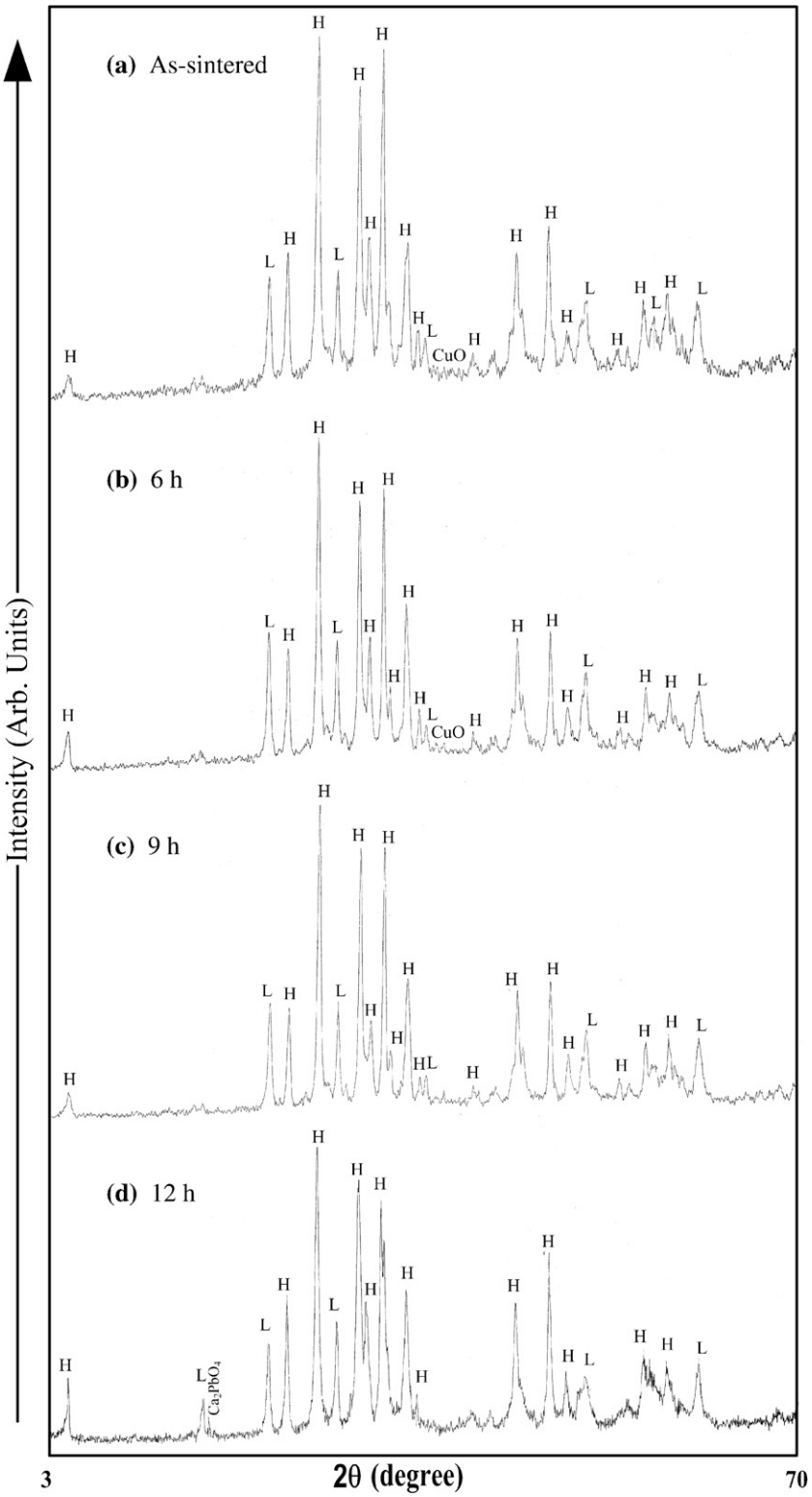

Fig. 1. (a–d) X-ray diffraction patterns of $Bi_4Sr_3Ca_3Cu_6O_x$ at different vacuum annealing time (0.0, 6, 9 and 12 h).

high-T_c (2223) phase. Otherwise, one can infer that at an annealing time equal to 9 h, the extent of outgoing oxygen from this sample is greater than for samples annealed at any other time. When annealing is continued further, i.e., 12 h in Fig. 1(d), it can be noticed that the intensity of the diffraction peaks of the high-T_c phase start degrading, decreasing the value of T_c, while the peak of the low-T_c phase slightly increases at $2\Theta = 29.2°$. It is peculiar also to note the existence of the insulating phase Ca_2PbO_4 at $2\Theta = 18.06°$ though in small quantities.

A closer examination of the XRD pattern also reveals another important feature of the two superconducting phases. Firstly, it is observed that the peaks of the high-T_c phase are sharpest at the stage when T_c has its maximum value of 102 K. At annealing periods less and also greater than this optimized time the peaks are relatively broad. Secondly, the peaks due to the high-T_c phase are relatively sharper than are the peaks due to the low-T_c phase. These observations indicate the distorted nature of the low-T_c phase and show the best crystallinity when maximum T_c is attained for the high-T_c phase.

3.2. Electrical properties

The electrical features of the samples were examined by resistivity versus temperature measurements (ρ–T). Fig. 2 depicts typical electrical resistivity as a function of temperature for the $Bi_4Sr_3Ca_3Cu_6O_x$ samples (as-sintered and annealed at 850 °C with evacuation at 10^{-2} Torr for 3, 6, 9, and 12 h). In Fig. 2, the as-sintered sample exhibits a semiconducting character in the 300–138 K region. Below 138 K, the resistivity decreases gradually with decreasing temperature and reaches a zero-value at a critical transition temperature $T_c \approx 77$ K. After vacuum annealed for 3 h, the electrical behavior started to change. As seen in Fig. 2, a metallic behavior was obtained from 300 K up 123 K, After $T^{ons} \approx 123$ K, the resistivity–temperature plot deviates from linearity and exhibits a noticeable resistivity drop with a small tail extending to the zero-resistivity state at $T_c \approx 83$ K. With prolongation of annealing time to 6 h, similar metallic behavior was observed, the T^{ons} value was found to be 116 K which is lower than for the above annealing period and T_c was found to be 90 K, which is higher than for $t_{ann} = 3$ h. With more prolongation of annealing time to 9 h, the annealed sample exhibits a remarkable resistive behavior compared with $t_{ann} = 6$ h. The resistivity curve shows an almost complete transition at $T^{ons} \approx 110$ K and a T_c value of 102 K, i.e., the prolonged vacuum annealing time up to 9 h appears to enhance the superconducting property. This behavior suggests that the 9 h annealed sample has a high fraction of the high-T_c phase (2223). This result is also supported by XRD analysis. For the longest period of vacuum annealing, 12 h, the temperature behavior of ρ is qualitatively similar to the former annealing time 9 h but with higher values of ρ and a lower value of $T_c \approx 89$ K. This trend may be ascribed to structural defects, like variable metallic ordering patterns. Such effects could be related to the lowering of the transition temperature T_c. In general, we can infer that there are many oxygen vacancies in the as-sintered sample, which causes a structural disorder in the Bi–O sheets, by which many electrons are localized and the superconductivity is partially degraded. As a result T_c was depressed. However, it can be decided that vacuum heat treatment for narrow steps of time (3–9 h) leads to excess oxygen vacancies moving out the sample, and the moving of oxygen enhances the arrangement of the lattice and produces the carriers which are responsible for better superconducting properties. Under our experimental conditions, it can be concluded that as the excess of oxygen moves out the metallicity of the Bi–O layers increases and consequently the values of T_c is enhanced.

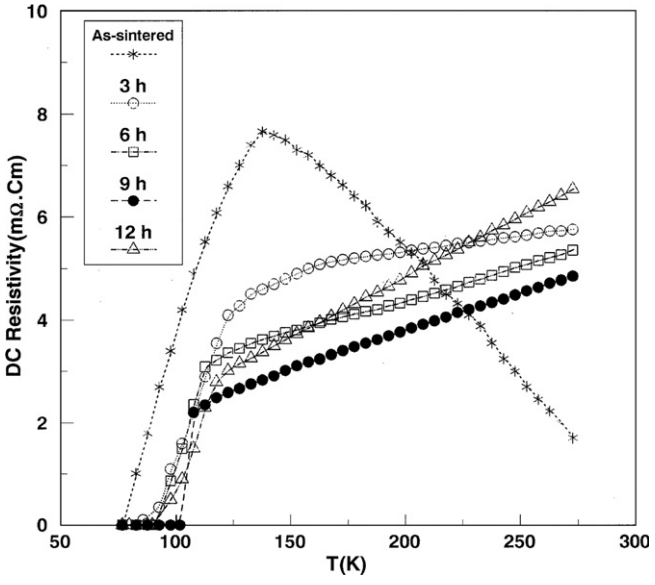

Fig. 2. Influence of vacuum annealing time on d–c resistivity of the nominal composition $Bi_4Sr_3Ca_3Cu_6O_x$.

It is worth mentioning that, we have made two important points here; firstly, by prolongation of vacuum annealing time, the superconducting phase coherence is enhanced. In particular, growth of superconducting phases, such as 2223 and 2212 phase is believed to be responsible for enhancement of superconducting properties. Secondly, excess oxygen in the Bi–O layers may enhance the square planar like arrangement around the copper ions and in turn the superconducting properties are enhanced. From the above results, one can easily deduce that the optimal annealing time = 9 h exhibits the best superconducting properties. Therefore, the in order to test the linear behavior of $\rho(T)$ at normal state, an expression of the form:

$$\rho(T) = AT + B \tag{2}$$

has been applied to the annealed samples in the temperature range between 130 and 300 K. The parameter "A" can be considered as the temperature coefficient of resistivity in the normal state with a value in the range 10^{-5}–$10^{-6}\,\Omega\,cm\,k^{-1}$ which is usually obtained for high-T_c superconductors [20,21]. The parameter "B" represents the residual resistivity (the value of $\rho(T)$ at $T = 0.0$) and has a value in the range of 10^{-3}–$10^{-4}\,\Omega\,cm$ which agrees with values usually obtained for high-T_c superconductors [22,23]. The effect of vacuum annealing time on the $\rho(T)$ dependence of the $Bi_4Sr_3Ca_3Cu_6O_x$ is given in Fig. 3. It can be observed that for all times of annealing, the range above T^{ons} is characterized by metallic behavior as usual for high-T_c superconducting materials. The transition to the superconducting state could be held at all times of

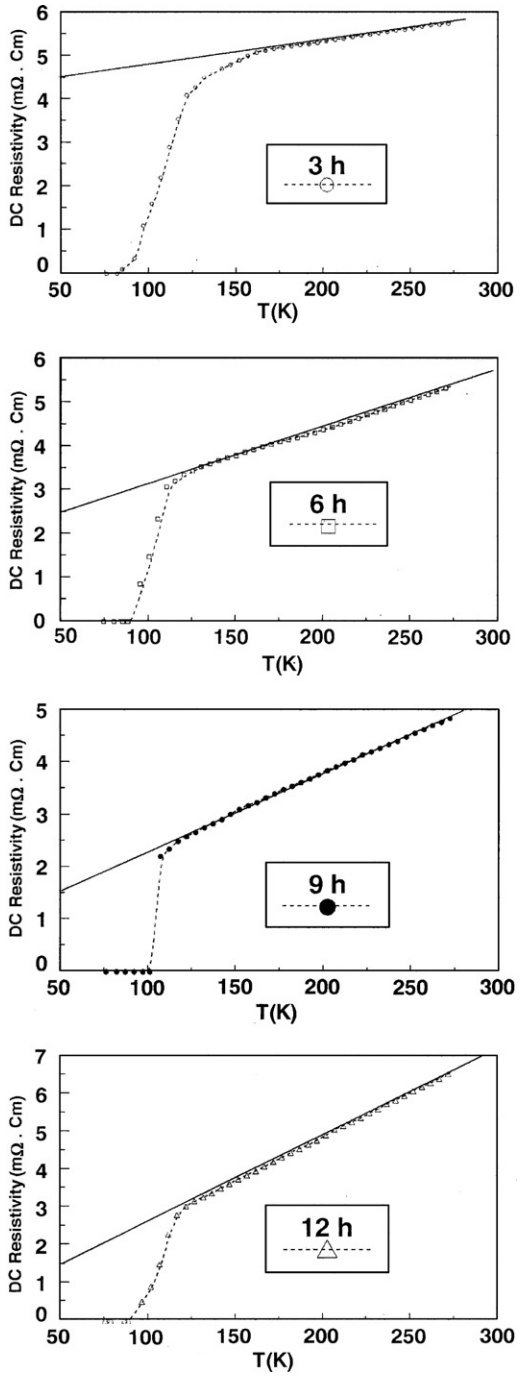

Fig. 3. Temperature dependence of resistivity of $Bi_4Sr_3Ca_3Cu_6O_x$ samples vacuum annealed for different annealing times. The straight lines are the fits of $\rho(T) = a + bT$ above $2T_c$.

annealing. The shortest period of vacuum annealing (3 h) was terminated by a short tail, confirming the role of impurities as has been confirmed by the XRD analysis, while, the most convenient time of vacuum annealing (9 h) was characterized by no tail. The variation of values of the parameters of Eq. (2), "A and B", with the time of vacuum annealing is given in Table 1. It is found that "A" increases from 0.61×10^{-5} to 2.27×10^{-5} with prolongation of annealing time (3–12 h), which is in good agreement with

Table 1
Variation of the normal and superconducting parameters obtained from the $\rho(T)$ measurements with the time of vacuum annealing of $Bi_4Sr_3Ca_3Cu_6O_x$

t_{ann}/h	3	6	9	12
$A \times 10^{-5}$ (Ω cm k^{-1})	0.61	1.27	1.35	2.27
$B \times 10^{-4}$ (Ω cm)	45	25	15	16
T^{ons} (K)	123	116	110	118
T_c (K)	83	90	102	89
ΔT (K)	40	26	8	29
$\rho_{273} \times 10^{-3}$ (Ω cm)	5.75	5.35	4.84	6.53

results obtained for similar high-T_c superconductors materials [20,21]. On the other hand, the parameter "B" decreases from 45×10^{-4} to 15×10^{-4} with prolongation of annealing time up to 9 h, then increases with more prolongation of $t_{ann} = 12$ h. The decrease in the value of "B" reflects relatively constant impurity levels or nonsuperconducting phases, which is a matter that could be confirmed by the XRD data. However, the values of "B" still agree with those usually obtained for high-T_c superconductors [23].

3.3. SEM observation

To look into the morphology, we have performed scanning electron microscopy on the vacuum annealed sample. Fig. 4 shows a micrograph of a pellet with a maximum value of $T_c = 102$ K. A plate-like phase seems to dominate the microstructure at this stage of annealing (9 h). Good quality plate-like crystals, quite moderate in size and relatively oriented, constitute the major phase giving rise to superconductivity [6]. Generally, it can be decided that, the vacuum annealing process plays a striking role in the changes of the physical appearance of the pellet.

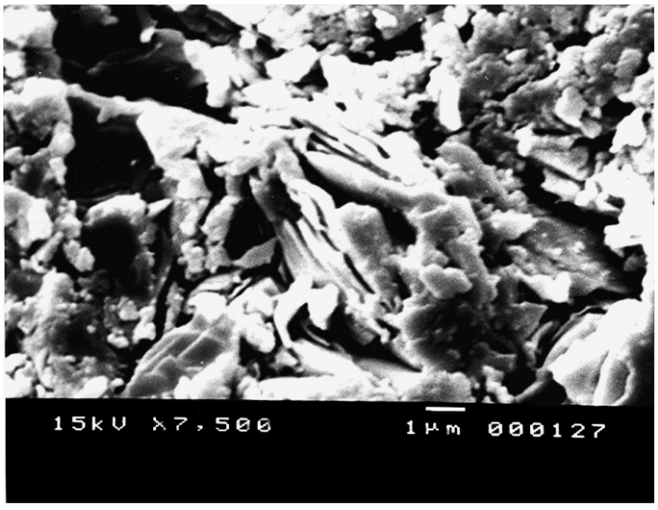

Fig. 4. SEM micrograph of the surface for the $Bi_4Sr_3Ca_3Cu_6O_x$ (vacuum annealed for 9 h).

3.4. Microhardness and density measurements

The effect of vacuum annealing time at (850 °C) for periods (3, 6, 9, and 12 h) on the Vickers microhardness (VHN) of the $Bi_4Sr_3Ca_3Cu_6O_x$ sample was examined. Fig. 5 depicts the variation of measured microhardness (VHN) against the vacuum annealing time at certain applied loads ($P = 0.25$, 0.49, 0.98, 1.96 and 2.94 N). It can be observed that at all applied loads the variation of VHN exhibits an ellipse-shape type behavior with an apex at annealing time (t_{ann}) = 9 h and a trough at $t_{ann} = 12$ h. The tremendous increase of VHN values from 1.09 GPa (0.245 N) at $t_{ann} = 3$–1.92 GPa (0.245 N) at $t_{ann} = 9$ h is ascribed to the formation of good conducting channels between superconducting grains which can enhances the bridging between them. This is most probably the reason for the high values of VHN. Furthermore, the annealing process improves the thermal conduction and, hence, stabilizes the temperature distribution between superconducting grains. The monotonic decrease of VHN values 1.00 GPa (0.245 N) at $t_{ann} = 12$ h can be a consequence of the partial dissolution of superconducting (metallic) phases. Also, the prolongation of annealing time (12 h) may generate circumferential cracks. Therefore, the contact between grains weakens, consequently lowering the values of VHN. Fig. 6 displays the change of VHN values with the applied load at $t_{ann} = 0$, 3, 6, 9, and 12 h. The curves in the graph show that disregarding the time of annealing the microhardness values decrease non-linearly as the applied load increases up to 0.980 N, thereafter, the VHN values tend to attain saturation. This type of non-linear behavior has also been observed in the literature for several kinds of materials and is termed an indentation size effect (ISE) [24–31]. The ISE behavior can be explained qualitatively on the basis of penetration depth of the indenter. Since the indenter penetrates only surface layers at small loads, the surface effect is more pronounced at these loads. However, as the depth of penetration increases, the effect of inner layers becomes more and more prominent and ultimately there is no change

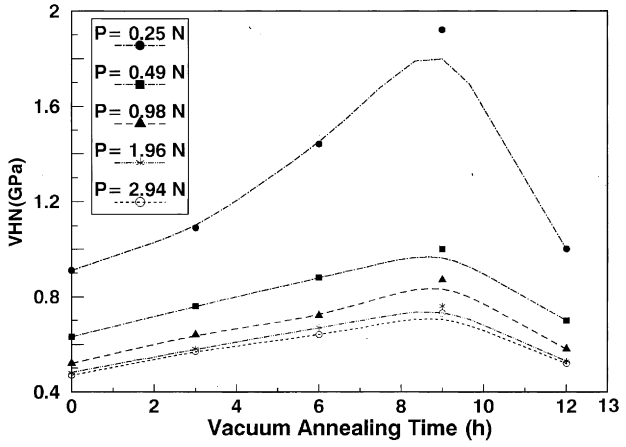

Fig. 5. The variation of microhardness with vacuum annealing time for the nominal composition $Bi_4Sr_3Ca_3Cu_6O_x$.

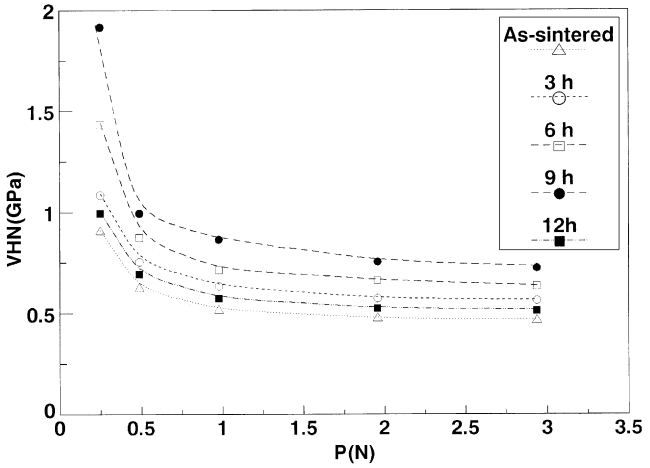

Fig. 6. The variation of microhardness with applied load for the nominal composition $Bi_4Sr_3Ca_3Cu_6O_x$.

in the value of the hardness with load. The measured indentation diagonal lengths and calculated microhardness values for different applied loads are given in Table 2 for each period of annealing time.

In order to describe the ISE behavior of materials, several relationships between the applied test load "P" and indentation diagonal length "d" have been given in the literature. The simplest way to describe the ISE is Meyer's Law (1908) [25,26]

$$\mathrm{Log}P = n\,\mathrm{Log}d + \mathrm{Log}K \tag{3}$$

where "n" is the Meyer number (or index) and "K" is the standard hardness constant. The values of Meyer's index n are used as a measure of ISE. When $n < 2$, the hardness increases with decreasing applied load, which is termed normal ISE. When $n > 2$ the hardness values increase with increasing applied load which is called reverse ISE. When $n = 2$, the hardness is independent of applied load. However, the exponent n has values greater or lower than 2 in most cases. The values of n and K in Eq. (3) may be obtained from the plots of $\mathrm{Ln}P$ against $\mathrm{Ln}d$. Typical plots of the dependence of $\mathrm{Ln}P$ and $\mathrm{Ln}d$ for BSCCO samples at $t_{ann} = 0$, 3, 6, 9 and 12 h are shown in Fig. 7. The determined n values obtained from the slopes of the best-fit lines in this figure are tabulated in Table 3. From Table 3, it can be noticed that n values vary from 1.44 to 1.58. These values of n indicate that Meyer's Law is obeyed in our results. On the other hand, the obtained results from Table 3 indicate that the load independent hardness values are lower than those of the conventionally estimated ones (Table 2). This observation is in agreement with experimental results in the literature [24,32].

Fig. 8 shows the apparent density change with increasing vacuum annealing time for the $Bi_4Sr_3Ca_3Cu_6O_x$ samples. One can easily observed that the measured density increases with increasing annealing time and has a peak at $t_{ann} = 9$ h. This observation can be attributed to the fact that the prolongation of vacuum annealing time increases

Table 2
Measured diagonal lengths and calculated microhardness values of $Bi_4Sr_3Ca_3Cu_6O_x$ samples for different applied loads

Applied load (N)	As-sintered		t_{ann}/h = 3		t_{ann}/h = 6		t_{ann}/h = 9		t_{ann}/h = 12	
	d (μm)	VHN (GPa)	d (μm)	VHN (GPa)	d (μm)	VHN (GPa)	d (μm)	VHN (GPa)	d (μm)	VHN (GPa)
0.245	22.3	0.91	20.4	1.09	17.8	1.44	15.5	1.92	21.5	1.00
0.49	38	0.63	34.6	0.76	32.1	0.88	30.1	1.00	36.03	0.7
0.980	59.1	0.52	53.3	0.64	50.2	0.72	45.7	0.87	56	0.58
1.96	87	0.48	79.2	0.58	73.7	0.67	69.2	0.76	82.8	0.53
2.94	107.7	0.47	97.8	0.57	92.3	0.64	86.4	0.73	102.4	0.52

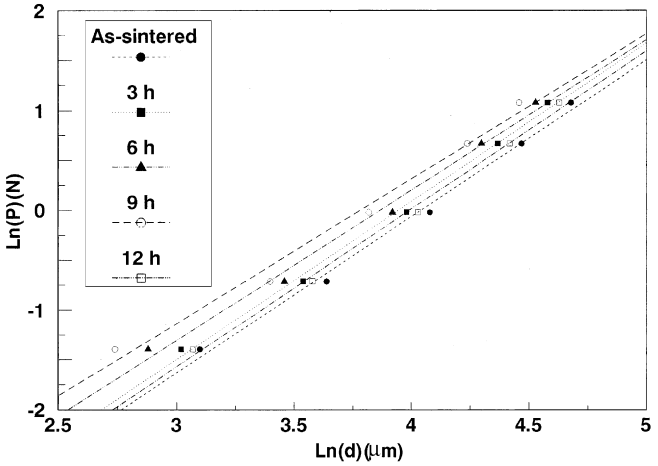

Fig. 7. The applied load Ln P with the Vickers diagonal Ln d for the nominal composition $Bi_4Sr_3Ca_3Cu_6O_x$.

Table 3
Hardness analysis results of $Bi_4Sr_3Ca_3Cu_6O_x$ samples for Meyer's Law

t_{ann}/h	n	K (GPa)
0.0	1.57	0.66
3	1.58	0.85
6	1.50	1.72
9	1.44	3.22
12	1.58	0.72

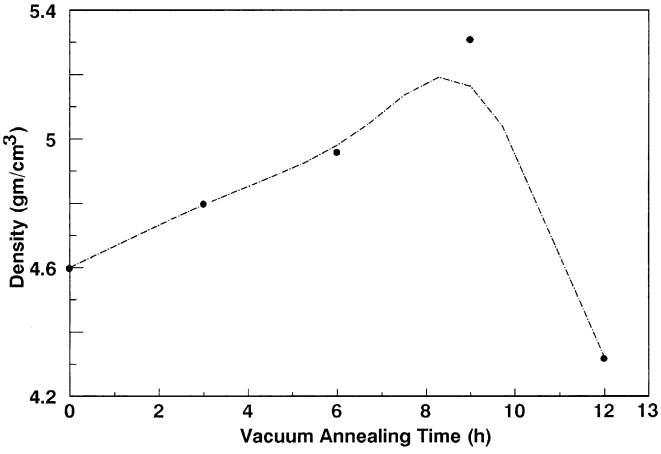

Fig. 8. The variation of density with vacuum annealing time for the nominal composition $Bi_4Sr_3Ca_3Cu_6O_x$.

the ability of the 2223 lattice for a favorable rearrangement, which leads to the increased density value [33]. Also, the enhancement of density is due to an increase in the long-range order of the crystal structure of annealed samples [34]. The measured density decrease after the peak is likely due to an increase of the hole concentration [35]. On the other hand, the density deficiency results from the decrease of structural symmetry and the degree of ordering. Generally, one can easily deduce that the mechanical properties are strongly affected by the macroscopic structural symmetry, oxygen content, and degree of ordering.

4. Concluding remarks

In conclusion we formulate the following points as below:

1. X-ray diffraction analysis suggests that the domination of the high-T_c phase (2223) increases as vacuum annealing time increases and that the optimal annealing time with $t_{ann} = 9$ h produces a nearly pure Bi-2223 phase.
2. Vacuum annealing treatment causes an increase in the metallicity of the Bi–O layers and in turn the values of T_c are enhanced.
3. SEM observations reveal that the sample with optimal vacuum annealing time $t_{ann} = 9$ h has good quality plate-like crystals that are quite moderate in size and relatively oriented.
4. Vacuum annealing treatment has a significant effect on increasing the hardness. This high hardness can be attributed to improvement of the thermal conduction and hence stabilization of the temperature distribution between superconducting grains.
5. The measured microhardness values of the BSCCO materials are load dependent. The variation of microhardness with load is non-linear. This observation is related to the indentation size effect (ISE).
6. Vacuum annealing conditions lead to a substantial increase of the sample density. This increase is owing to long-range ordering of the sample's crystal structure.

References

[1] H. Maeda, Y. Tanaka, M. Fukumoti, T. Asano, Jpn. J. Appl. Phys. 27 (1988) L290.
[2] J.L. Tallon, R.J. Buckley, P.W. Gilberd, R.M. Presland, I.W.M. Brown, M.E. Bowder, L.A. Dwistian, R. Goguel, Nature 333 (1988) 153.

[3] S.M. Khalil, A. Sedky, Physica B 357 (2005) 299.
[4] A.K. Sarker, I. Maartese, Physica C 168 (1990) 591.
[5] S.M. Khalil, Phys. Status Solidi A 178 (2000) 731.
[6] S. Chandra, S.A. Agnihotry, P. Asthana, K.C. Nagpal, K.K. Saini, Chanderkant, C.P. Sharma, S.N. Ekbote, Phys. Status Solidi A 123 (1991) 269.
[7] D. Bahadur, A. Banerjee, A. Das, K.P. Gupta, A. Mitra, M. Tewari, A.K. Majumdar, J. Mater. Sci. 25 (1990) 4852.
[8] L. Shi, Q. Dong, Y. Zhang, Physica C 341–348 (2000) 649.
[9] J. Wang, M. Wakata, T. Kaneko, S. Takano, H. Yamauchi, Physica C 208 (1993) 323.
[10] Huey-Chuen I. Kao, Nien-Hour Wang, Chi-Ming Wang, Physica C 185–189 (1991) 839.
[11] R. Rajput, Y.S. Reddy, D.P. Singh, K.D. Kundra, R.G. Sharma, Solid State Commun. 79 (1991) 667.
[12] T.K. Bansal, S. Bansal, R.L. McGreevy, S.H. Smith, G. Garton, Appl. Phys. Lett. 53 (21) (1988) 2093.
[13] Y. Kimishima, J. Nakano, Physica C 185–189 (1991) 835.
[14] J. Joo, J.P. Singh, R.B. Poeppel, presented at High-T_c Superconductors, 1991 Fall Meeting of Mater. Res. Soc. Boston, December 2–6, 1991.
[15] D.W. Johnson Jr., W.W. Rhodes, J. Am. Ceram. Soc. 72 (12) (1989) 1346.
[16] S.M. Khalil, Smart Mater. Struct. 14 (2005) 804.
[17] S.M. Khalil, J. Phys. Chem. Solids 62 (2001) 457.
[18] M.M. Ibrahim, S.M. Khalil, A.M. Ahmed, J. Phys. Chem. Solids 61 (2000) 1553.
[19] S.M. Khalil, J. Phys. Chem. Solids 64 (2003) 855.
[20] A.V. Pobe, G.H. Ilonca, D. Ciurchea, V. Pop, A. Konopko, I.I. Gerue, M. Todica, V. Ioncu, Int. J. Mod. Phys. B 9 (1995) 695.
[21] S.V. Sharma, G. Sinha, T.K. Nath, S. Chakraborty, A.K. Majumdar, Physica C 242 (1995) 351.
[22] L. Navarrete, A. Sanchez, A. Marino, Physica C 235–240 (1994) 1943.
[23] S.H. Han, O. Rap, Solid State Commun. 94 (1995) 661.
[24] U. Kölemen, O. Uzun, M. Yilmazlar, N. Güçlü, E. Yanmaz, J. Alloys Compds. 415 (2006) 300.
[25] K. Sangwal, B. Surowska, Mater. Res. Innov. 7 (2003) 91.
[26] R. Tickoo, R.P. Tandon, K.K. Bamzai, P.N. Kotru, Mater. Chem. Phys. 80 (2003) 446.
[27] A.A. Elmustafa, D.S. Stone, J. Mech. Phys. Solid 51 (2003) 357.
[28] O. Uzun, U. Kölemen, S. çelebi, N. Güçlü, J. Eur. Ceram. Soc. 25 (2005) 969.
[29] O. Uzun, T. Karaaslan, M. Gogebakan, M. Keskin, J. Alloys Compds. 376 (2004) 149.
[30] K. Sangwal, B. Surowska, P. Blaziak, Mater. Chem. Phys. 80 (2003) 428.
[31] J. Gong, H. Maio, Z. Peng, L. Qi, Mater. Sci. Eng. A 354 (2003) 140.
[32] A.K. Dutta, N. Narasaiah, A.B. Chattopathyaya, K.K. Ray, Ceram. Int. 27 (2001) 407.
[33] S.V. Lubenets, V.D. Natsik, L.S. Fomenko, Low. Temp. Phys. 30 (2004) 345.
[34] A. Tampieri, R. Masini, L. Dimesso, S. Guicciardi, M.C. Malpezzi, Jpn. J. Appl. Phys. 32 (1993) 4490.
[35] Y. Shimakawa, Y. Kubo, T. Manako, T. Satoh, S. Iijima, T. Ichihashi, H. Igarashi, Physica C 157 (1989) 279.